Final Draft
of the original manuscript

Shariati, M.; Weber, W.; Bohlen, J.; Kurz, G.; Letzig, D.; Höche, D.:

Enabling intelligent Mg-sheet processing utilizing efficient machine-learning algorithm.

Enabling intelligent Mg-sheet processing utilizing efficient machine-learning algorithm[⋆]

Mohamadreza Shariati[a,*], Wolfgang E. Weber[a], Jan Bohlen[b], Gerrit Kurz[b], Dietmar Letzig[b] and Daniel Höche[b,**]

[a]*Chair of Structural Analysis,* Helmut-Schmidt-*University / University of the Federal Armed Forces Hamburg, D-22043 Hamburg, Germany*
[b]*MagIC - Magnesium Innovation Centre, Institute of Materials Research* Helmholtz-*Zentrum Geesthacht, D-21502 Geesthacht, Germany*

ARTICLE INFO

ABSTRACT

Process - property relationship control during magnesium sheet manufacturing is demanding due to the complexity of involved physical parameters and the sensitivity of the system to small changes. Here, data science might help to extract crucial information on interdependencies between processing parameters and sheet quality. In this paper we suggest a dedicated machine learning framework, which enables the possibility of correlating material property determining concepts such as pole figure to processing parameters, namely temperature and deformation degree without knowledge on prior dependencies of physical variables. Despite the impacts that using a relatively small data set can have, for Mg-AZ31 alloy we show that some projections of crystallographic texture can be reliably predicted from mechanical measurement data set. In general, the framework is useful for those processing parameters, which conventionally can be represented by a mathematical basis in the context of interpolation. In the future with access to more data it is proposed that applying our approach might allow predicting and controlling in-situ the rolling process route.

1. Introduction

Currently, magnesium based materials are used for lightweight components in vehicles, for biomedical applications or are handled as candidate to become anode material for post-Li energy storage devices. Most common in the automotive sector is the processing as die castings. Die casting allows the fabrication of components with a complex geometry. Nevertheless, the mechanical properties of the die cast components often do not meet essential requirements with regard to endurance, strength, ductility, etc. A promising alternative for thin, large area parts, such as automotive body components, are components made from magnesium sheets. Relevant deep drawn parts are characterized by high quality surfaces without pores and superior mechanical properties in comparison to die cast components. However, this requires production of high-performance dies, as shown by a promising approach by e. g. Curbach et al. [12]. To bring magnesium sheet components or even Mg-foils for future energy applications to the market, it will be necessary to fabricate material with competitive properties in an economic production process. A favored processing route for the production of magnesium sheets is a two step process. The first step is the production of thin strips by twin-roll casting (TRC) [3]. In the second step these strips will be rolled to final gauge in a conventional rolling process. Twin-roll casting of thin strips combines solidification and rolling into one single production step. Thus, it saves a high number of rolling and annealing passes in comparison to the conventional rolling process from the slab [20, 18, 11, 22, 1]. The

impact of process parameters of twin roll cast strip properties is described elsewhere [14]. The strips produced by twin-roll casting are used as feedstock material in subsequent rolling process. The conventional rolling process represents the established production method for the manufacturing of sheets. The used feedstock material is passed through a pair of rolls, whereby the roll gap remains smaller than the thickness of the feedstock, such that plastic deformation occurs. The sheet properties, e. g. the mechanical properties, can be related to the applied rolling process parameters, a sequence of individual hot rolling passes followed by a heating phase [5]. The rolling temperature is an essential process parameter, which e. g. activates important deformation and recrystallization mechanisms in Mg alloys. A coarser grained microstructure is obtained at higher rolling temperatures as a result of dynamic recrystallization and grain growth [17]. Furthermore, the texture weakness i. e. the significance of alignment of the basal planes in the sheet plane decreases with increasing rolling temperature [6, 17, 10]. The degree of deformation (i. e. the amount of plastic strain in the thickness direction) per rolling pass also influences the microstructure and texture, as it determines the strain rate and the extent of deformation before recrystallization of the deformed microstructure during intermediate annealing [9].

In sheet rolling procedures, experiments are rather complex and time consuming. Therefore the amount of data for a single alloy is always quite limited. This paper reports on results of rolling experiments on twin-roll cast strips of magnesium alloy AZ31 (Mg-3Al-1Zn-Mn) with the rolling parameters degree of deformation ϕ and temperature T. Herein, the degree of deformation ϕ is equal to the plastic strain in the thickness-direction of the metal sheet. Aspects of non-uniform deformation are neglected.

It will be shown that despite the complex interdependen-

cies of involved physical parameters, the proposed machine learning framework enables process control within a manufacturing data space. In the future the data space might be applied to control actors within an intelligent sheet manufacturing route.
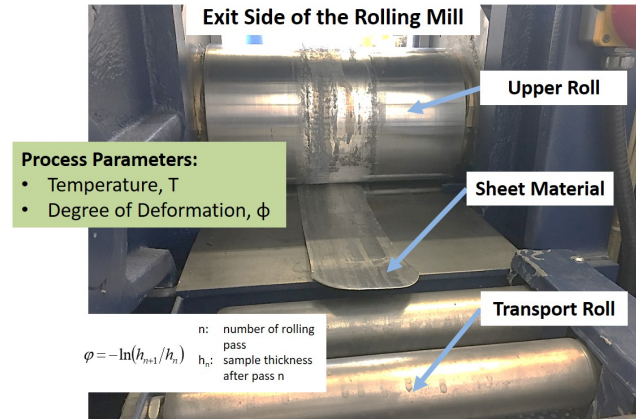

Figure 1: Varied process parameters, rolling temperature T and degree of deformation ϕ

2. Experimental testing and (training) data generation

2.1. Rolling of magnesium sheets

For the rolling trials, twin-roll cast feedstock material of the commercial magnesium alloy AZ31 produced in one batch was used. All strips had a width of 350 mm, an initial thickness of approx. 5.6 mm and are twin-roll cast at a temperature T of 650 °C with a casting speed of 1.8 m/min, [15]. For rolling the AZ31 strip was used in the as-twin-roll cast condition and rolled at three different rolling temperatures, 350 °C, 400 °C, and 450 °C, as well as three different degrees of deformation per pass, $\phi = 0.1$, $\phi = 0.2$, and $\phi = 0.3$, to a final gauge of 2 to 2.1 mm [15]. Prior to the rolling procedure the strips were heated for 30 min to the respective rolling temperature. Between the following rolling passes, the rolled samples were again reheated to the rolling temperature for 15 min. After the final rolling pass the sheets were air cooled. The rolling speed was 10 m/min and a water-soluble oil based lubricant was used. Not considering the influence of variation of other TRC parameters is justified by the optimization history of the parameter space at the facilities.

2.2. Micrographs and texture measurements

After rolling, the microstructures of the materials were analyzed using optical microscopy. Standard metallographic sample preparation techniques were employed and an etchant based on picric acid was used to reveal grains and grain boundaries, [13]. Texture measurements in the sheets were performed on the sheet mid-planes using a Panalytical X-ray diffractometer setup and CuK_α radiation. Six pole figures were measured up to a tilt of 70° which allows recalculation

of full pole figures using the open source software routine MTEX, see e. g. [2]. The (0001) pole figure is used in this work to present the texture of the sheets at the midplane. This simplification of texture presentation appears worthwhile, as the angular distribution of basal planes has been shown to have the most significant impact on the mechanical behaviour due to easy activation of basal slip.

2.3. Mechanical testing

In order to see how the different process parameters do influence the mechanical properties of the sheets, stress-strain curves were measured by tensile tests according to DIN EN 10002. Testing was performed on samples extracted from the sheet in rolling direction, 45° to rolling direction and in the transverse direction. For statistical verification, 4 tensile tests were performed per test parameter. Curves were analyzed according to mechanical standards for tensile yield strength (TYS), ultimate tensile strength (UTS) and elongation at fracture (A).

3. Data and data analysis

3.1. Experimental data

Figure 2 displays the microstructures from longitudinal sections of the as-rolled sheets of alloy AZ31. The microstructures of all sheets are not fully recrystallized. With increasing rolling temperature the amount and size of the not recrystallized grains decreases, see e. g. [15]. The sheets rolled at 450 °C with the degree of deformation of $\phi = 0.1$ are nearly fully recrystallized, [15]. With increasing degree of deformation the amount and size of the deformed grains are increasing again. In the sheets rolled at 350 °C and a degree of deformation of $\phi = 0.3$ shear bands are observed [15]. Consequently, two process control variables are chosen to be implemented as part of the manufacturing data space:

- Data for the data space: T, ϕ

For the texture development it is known that it remains rather uniform in comparison to other alloy series. The basal planes are basically aligned to the sheet surface with a tilt towards rolling direction (RD) or transversal direction (TD) with different significance. A special resulting aspect is the development of a split peak component with tilt to RD. The (0001) pole figures (basis plane defined via x and y coordinates) of nearly all the sheets show detectable pronounced split peaks towards the rolling direction and an angular distribution to the transverse direction, cf. [15]. This texture can be associated to the high amount of unrecrystallized grains in the rolled material [21]. Because of this effect the (0001) pole figure of the sheet rolled at 450 °C and a degree of deformation of $\phi = 0.1$ show a single peak, see [15]. The tendency to develop such a texture increases with increasing rolling temperature and decreasing degree of deformation per pass and is consistent with further recrystallized microstructures, see e. g. [15]. For the manufacturing data space we reduce the amount of data describing the intensity $I_{0001}(x, y)$ of the pole figure by only using the two (or via
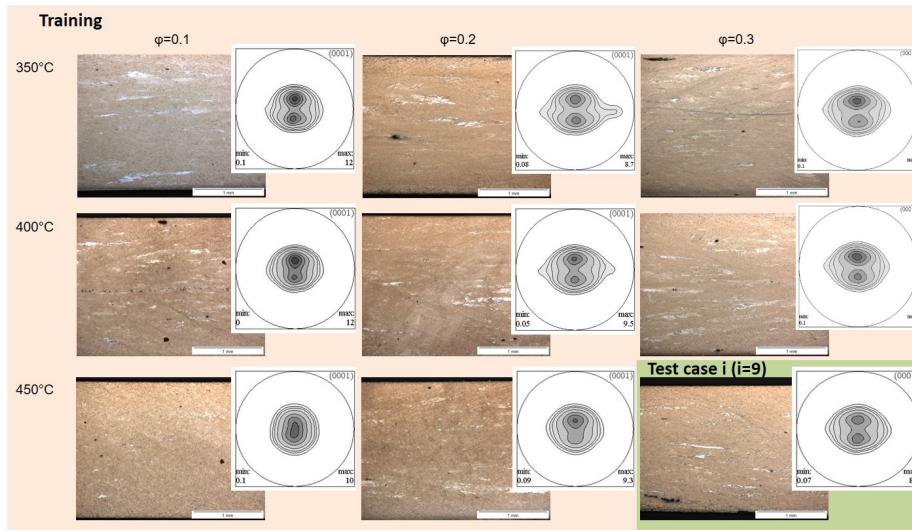
Figure 2: Cross-section micrograph and respective pole figures of (0001), taken from [15]. Usage of data in Section 3 is indicated

convolution – single) maxima values p_1, p_2 and by assuming single peak GAUSSian like profiles. Although we are aware that an approximation of this texture with the used GAUSSian fit curves is far away from an appropriate texture description, the main aspect of the textures which is also relevant for the activation of the underlying deformation mechanism is well featured. Any alloy which does not reveal a comparable texture will not be described in this way but this first approach with simple parametrization can be used for the description of AZ31. As there is no physical meaning of the position of the higher peak maximum (depends on the sample placement direction within XRD machine) it is allowed to define an additional constraint to lower the final error:

- Data for the data space: $I_{0001-1,2}$ maximum or in short form p_1, p_2 with $p_1 \geq p_2$ by definition
  (Remark: This approximation in general is not a valid texture description, however mathematically applicable for our use case.)

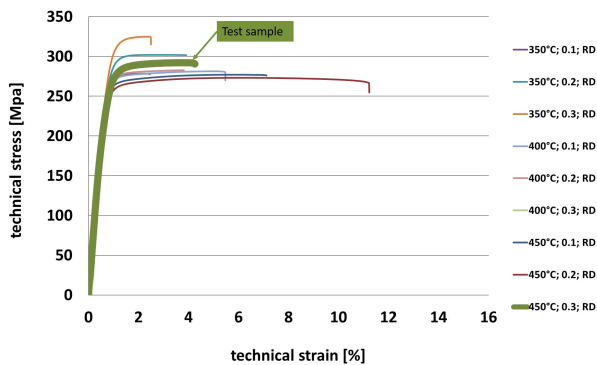Figure 3 displays the stress-strain curves of the speci-

men taken in the rolling direction, representative for all tensile tests. The stress-strain curves in Figure 3 respectively the data in Table 1 show in tendency that the elongation at fracture increases with increasing temperature, whereas the yield strength and ultimate tensile strength decrease. This tendency also corresponds to the stress-strain curves taken in transverse direction and 45° to the rolling direction, see e. g. [15]. This inverse behaviour can be observed at increasing degree of deformation. This material behavior is understood by a higher work hardening of the material at higher deformation degrees. At higher rolling temperatures recrystallization effects weaken the material hardening and lead to increased formability of the sheet material, i. e. the fracture strain in the context of this work, [15]. Therefore the entire mechanical property design space can be described by only three numbers per three cases determined by standard tensile testing according to DIN EN 10002.

- Data for the data space: TYS, UTS, and A in three directions (longitudinal, transverse, 45°) to rolling (given in Table 1)

In a data space of dimension 10 (T, ϕ, $I_{0001-1,2}$, TYS, UTS, A, three directions) with 9 original (and 41 regenerated) data points (40 for training and 1 for testing), the best possible process-structure property correlation with minimum error is targeted.

3.2. Feedforward Neural Network

In this study, we use the basic type of neural networks, namely, multi layer perceptron or multilayer feedforward network. These networks are known as a practical vehicle for performing a nonlinear input–output mapping of a general nature, [8]. Here, a mapping between processing parameters and mathematically representable property is sought. Mathematically representable means mechanical properties, in this case pole figure can be represented with a mathematical basis similar to well-known interpolation problems in

Figure 3: Stress strain curves in rolling direction (RD), taken from [15]

mathematics. For a neuron i, let $\{a_1, \ldots, a_m\}$ be outputs of neurons $1, \ldots, m$ in the previous layer, which are connected to neuron i with weights $\{w_{1i}, \ldots, w_{mi}\}$. The adder for summing the input signals to neuron i is defined as

$$\Sigma_i = \sum_{j=1}^{m} w_{ji} a_j + b_i \quad , \tag{1}$$

where $b_i \in \mathbb{R}$ is a bias. The bias is only added to the nodes in hidden layer. Its value is determined by the training procedure. Inclusion of a bias in our case, helps to contain shifts of the mapping we are replicating by the network. Additionally, because the network is fully connected, adding free parameter requires to add a neuron, which will contribute more than one weight to free parameters. Therefore adding a bias is a good way to add a single free parameter. The output of neuron i is computed by $f(\Sigma_i)$. The activation function $f(\cdot)$, considered to be a hyperbolic tangent sigmoid function of the form

$$f(\Sigma_i) = \frac{2}{1 + \exp(-2\Sigma_i)} - 1 \quad . \tag{2}$$

The mapping we want to replicate with the network is infinitely continuously differentiable in nature. Since the pole figure is tied to processing parameters based on [15]. However, in higher temperatures and with lower extend higher deformation degrees the change in texture development becomes less sensible. This choice of function serves this requirements. Note that in the both input and output layer, the neurons have identical activation functions. Assigning the input units, the output of the network can be calculated as a vector-valued function of N unknowns consist of connection weights and biases $F(u_1, \ldots, u_N; \vec{x})$ for an input vector $\vec{x}$. The dimension of function $F(\vec{u}; \vec{x})$ is equal to the number of outputs. In order to compute the network connection weights (learning step of the neural network), we use the BAYESian regularization method as it is discussed in [4]. Due to the scarcity of data in process-property problems, which is caused by resource consuming experiments, this learning method is strongly recommended. In fact, the BAYESian regularization method is considered to be a remedy to avoid over-fitting in regions of sparse data for classification problems [4]. In the conventional methods of feedforward network training, a vector $\vec{u}$ that minimizes the error function is found by suitable optimization method. On the other hand, in BAYESian regularization the unknown vector $\vec{u}$ is chosen from a prior distribution, then the most probable $\vec{u}$ is obtained by seeking minimum of the negative logarithm of the probability which is generally called an error function. The error function against the expected output y of the training set for BAYESian regularization is of the form

$$E(\vec{u}) = \frac{\beta}{2} \sum_{n=1}^{S} (F(\vec{u}; \vec{x}^n) - y^n)^2 + \frac{\alpha}{2} \|\vec{u}\|^2 \quad , \tag{3}$$

where S is the number of all training data points and α, β are hyperparameters for weights prior probabilities and variance of initial distribution for weights. In short, this learning method deals with data scarcity and over-fitting problem, besides, its probabilistic nature gives the most probable model with least complexity for the same performance. It is discussed in detail with an interpolation example in [4]. In order to minimize the error function (3), we use the well-known LEVENBERG-MARQUART algorithm that is endowed with GAUSS-NEWTON approximation to the HESSian matrix as introduced in [7]. The algorithm finds a local minimum for $\vec{u}$.

For the output, (0001) pole figure, we consider a convolution of two GAUSSian functions of the general form

$$\kappa(x, y) = \sum_{i=1}^{2} p_i \exp(-\frac{(x - x_i)^2}{2\sigma_{x,i}^2} - \frac{(y - y_i)^2}{2\sigma_{y,i}^2}) \quad , \tag{4}$$

where (x_i, y_i) is the CARTESian coordinate of center of GAUSSian i (x, y basis plane), p_i value of the pole maximum intensity, $\sigma_{x,i}$ and $\sigma_{y,i}$ are spread of the functions in direction x and y.

3.3. Data analysis

The dimension of data is 10. Since we use a relatively small set of data, at first, a dimensionality reduction is applied on the data.

To do this, the so called Local Linear Embedding (LLE) technique, first introduced in [19], is chosen by a neighborhood graph of size K. This technique is classified as a local nonlinear technique, which is promising compared to the traditional linear methods such as Principal Component and Linear Discriminant Analysis, cf. [16]. In order to keep the distance of data points, the technique preserves the manifold through neighborhood graphs. Preserving the manifold is of high importance in our study, since we look for the mapping from meaningful input parameters that in fact have a natural dependency. If the manifold changes, it means the natural dependency is changed. Another advantage is that, as a local technique, it allows for successful embedding of non-convex manifolds. The latter is also critical for our study, since we have no prior information over the manifold. The aimed dimension for dimensionality reduction is set 4. The result of Maximum Likelihood Estimator with and without temperature factor was 2.6. A choice of 4 rather than 3, seems to be an appropriate choice. To have a unique solution for dimensionality reduction as in ROWEIS et al. [19] the choice $K > 4$ for the graph is reasonable, since it results in a system with more equations than unknowns. We set $K = 5$ in our observations. To create more data points artificially, we set one data point aside for testing. Then the remaining data is regenerated 4 times with a maximum error bound of 1% that comes from a GAUSSian distribution. In this way we have 40 data entries for training and 1 data for testing. The amount of test data is very small. To tackle this we circulate the test data tag over data set and repeat the experiment including training step.

Table 1
Collection of sheet property data (TYS and UTS in [MPa], A in [%]
) based on stress-strain curve evaluation of data (D_i) according to Figure 3

degree of deformation data points (D_i)		$\phi = 0.1$			$\phi = 0.2$			$\phi = 0.3$		
		D_1	D_2	D_3	D_4	D_5	D_6	D_7	D_8	D_9
45°	TYS	219	227	231	243	222	216	239	222	237
	UTS	266	271	270	292	271	267	303	281	283
	A	6.27	7.22	6.56	5.62	7.24	11.54	5.37	8.14	8.83
transverse	TYS	214	227	226	236	220	217	234	221	223
	UTS	267	270	272	294	273	275	302	284	273
	A	2.59	1.93	2.57	1.55	1.79	4.85	2.34	3.27	2.95
longitudinal	TYS	261	260	252	274	252	240	284	258	250
	UTS	279	281	277	305	280	273	323	292	290
	A	1.76	4.86	6.72	3.38	3.46	10.57	1.91	2.77	4.99
temperature °C		350	400	450	350	400	450	350	400	450

A feedforward network with one hidden layer of size 4 is applied. The bias only exists on hidden layer and it is a vector in $\mathbb{R}^4$. The total number of unknowns is $4{\times}4+4{\times}2+4 = 28$. It equals to the number of connections between input and hidden layer and connections between hidden layer and output layer plus 4 biases in the hidden layer. The input and output data is normalized to $[-1, 1]$ automatically by the *feedforwardnet()* function in MATLAB. The GAUSSian functions of form Eq. (4) are simplified with $2\sigma^2_{x,i} = 0.25$, $2\sigma^2_{y,i} = 0.5$, $i = 1, 2$, $(x_1, y_1) = (1, 1.75)$, and $(x_2, y_2) = (1, 1.25)$. These texture fitting parameters impose the expected split of peaks in pole figure. p_1, p_2 are the network output data. With this setting shown in Fig. 4, we step forward to computation.

3.4. Implementation and Error analysis

MATLAB Deep Learning Toolbox^{TM} (formerly Neural Network Toolbox^{TM}) $R2019a$ is used for the implementation. It minimizes the error as given with Eq. (3) by the algorithm as documented in [7]. As discussed in 3.2 the training avoids over-fitting and results in a network that is generalized well. The search for the optimal solution of $\vec{u}$ and prior distributions, has a high dependency on the random seed. We observed that the error for the testing data point varies between different random seeds. In order to have a meaningful error analysis we consider

- A network is trained 500 times starting from a fixed random seed by using MATLAB function $rng(4e5)$. The error vector of the test is defined as

$$\begin{bmatrix} e_1 \\ e_2 \end{bmatrix} = \begin{bmatrix} e_1^j \\ e_2^j \end{bmatrix} \quad j := \min_i \max\{e_1^i, e_2^i\}, \quad i = 1, \dots, 500 \quad.$$

where at each experiment $i = 1, \dots, 500$, $e_1^i = |p_1 - p_1^i|$ and similarly $e_2^i = |p_2 - p_2^i|$.

- The relative error vector here is defined as

$$\begin{bmatrix} e_1^r \\ e_2^r \end{bmatrix} = \begin{bmatrix} e_1/I_1 \\ e_2/I_2 \end{bmatrix}$$

where

$$I_1 := \max_{D_i} p_1 - \min_{D_i} p_1$$

and similarly

$$I_2 := \max_{D_i} p_2 - \min_{D_i} p_2$$

.

- We use every data point once as the test and train the network with remaining 8 (after regeneration 40) data points. It gives a more comprehensive evaluation considering the data availability limitations.

The numerical result for experimental pole figure data points (p_1, p_2) from Figure 2 are as shown in Table 2. The experimental and predicted pole figures can be seen in Figure 5. The error bars in Figure 5 show the defined relative error for each data point. As it can be read from the Figure 5, the relative error is at its peak in D_1 and D_9. Interestingly at these points the minimum and maximum of temperature T and degree of deformation ϕ is attained, which are the two independent parameters in this experiment. From physical point of view, for the points D_1 and D_9 no information (data point) is available on respectively, lower and higher ϕ and T values. Naturally, the map at these points is not well presented and consequently, the network was not able to achieve better prediction. Nevertheless, the average relative error of all predictions is $\begin{bmatrix} 19.15\% \\ 17.15\% \end{bmatrix}$.

3.5. Manufacturing data space and testing

After the data space defined and the network has trained and tested for the cases shown in Figures 2, 3 the result in pole figure data is illustrated in Figure 5. The aim was to propose a machine learning framework for application within a sheet manufacturing route. The two GAUSSian peaks of $I_{0001}(p_1, p_2)$ were determined via experiment as shown in Table 2. Obviously, based on this very limited data set, the algorithm is capable to correctly predict pole figure data in most cases. The algorithm predicts on average with an error less than 20%. With respect to the very limited data
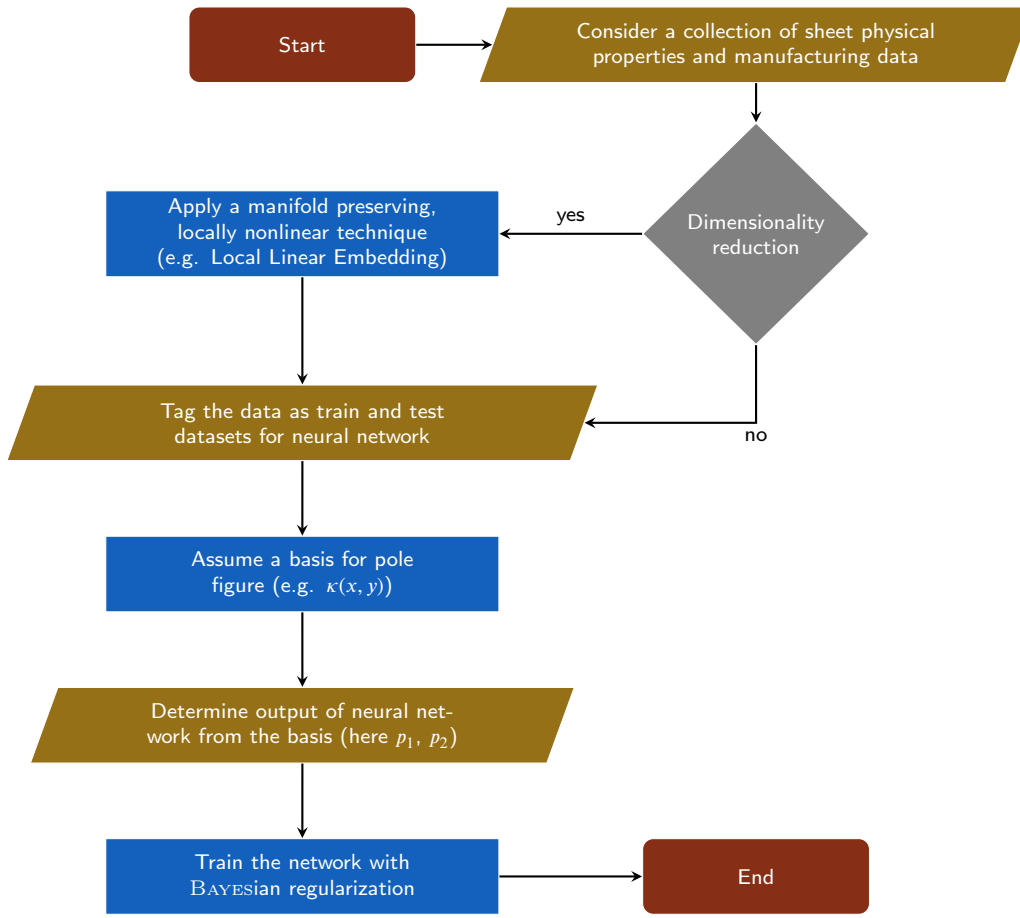
Figure 4: Proposed Machine Learning Algorithm

Table 2
Error of prediction for each data point as test

	D_1	D_2	D_3	D_4	D_5	D_6	D_7	D_8	D_9
p_1	12	12	10	10	9.5	9.3	8.7	10	8.7
p_1^j	13.08	10.91	9.25	9.09	10.12	9.33	9.83	9.6	10.05
e_1	1.08	1.09	0.75	0.91	0.62	0.03	1.13	0.4	1.35
p_2	10.3	9.2	9.7	7.6	8.0	7.2	8.5	8.0	8.6
p_2^j	9.09	10.41	9.1	8.51	8.2	7.25	8.85	8.24	9.83
e_2	1.21	1.21	0.6	0.91	0.2	0.05	0.35	0.24	1.23

space and consequent simplifications in GAUSSian function, the process-structure-property correlation is clear, however there is plenty of room to improve the accuracy. For a further reduction of error bounds, cost-effectiveness has to be taken into account, cf. [23]. To manage deviations at the boundary of the parameter window and to reduce errors additional training data is required. Indeed availability of data make it possible to include more free parameters in GAUSSian function (such as $\sigma_{x,i}$, $\sigma_{y,i}$, (x_i, y_i)) and determine them in the learning step. Application of more complex networks to improve the accuracy has discussed comprehensively in the field of machine learning. The complexity of network in the context of feedforward networks is obtained by adding more network unknowns, which requires more data points to yield a reliable solution. Another possible strategy for consider-

able improvement is change in mathematical basis which is the backbone of our algorithm. Applying functions other than GAUSSian function, that are more compatible with the nature of the pole figure or other property defining concepts can have a huge influence on better performance of proposed algorithm.

Figure 6 illustrates how the application of the algorithm simplifies the data space with D_9 as a representative test sample. The algorithm predicts $\begin{bmatrix} 10.1 \\ 9.8 \end{bmatrix}$ which is still in good agreement to the experimental values $\begin{bmatrix} 8.7 \\ 8.6 \end{bmatrix}$ despite the fact that the test data is allocated at the parameter window boundary. Tolerating a certain error bound, with a very limited manufacturing data space, the algorithm enables end-users
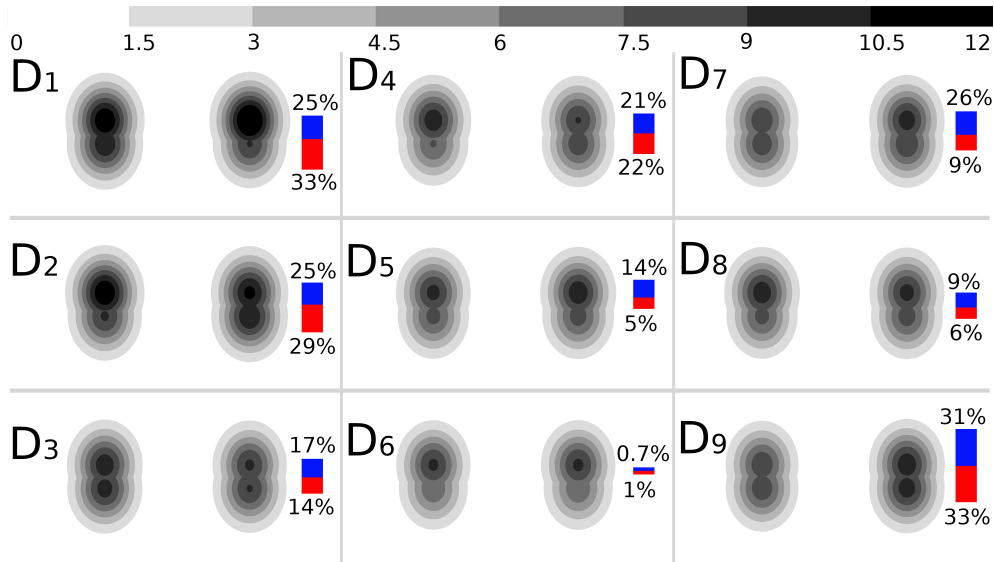
Figure 5: For each data point D_i experimental result at the left (targeted pole figure) vs. the algorithm based prediction at the right. The relative error is represented as red bar for the pole intensity p_1 and blue for p_2. Note that each column has fixed ϕ and each row fixed T.

to efficiently and fast adapt process parameters. In a prescriptive manner, it can be embedded within a software and actor control unit, in-situ for better intelligent processing. The capabilities of the algorithm and the efficiency in prediction and correlation might be extended by adding more data from literature, image analysis, monitoring data or materials / process simulations as indicated in Figure 6.
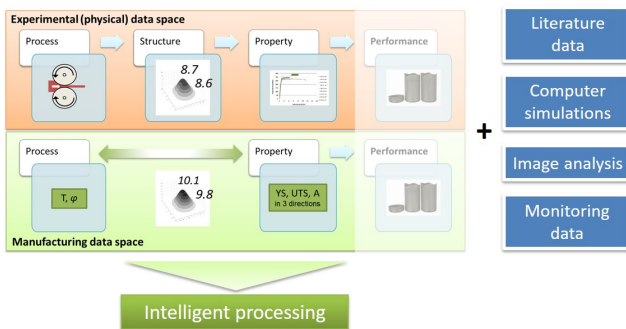

Figure 6: Condensing the huge experimental data space for wrought processing to a limited manufacturing data space enabling fast intelligent process adaption (here for example D_9). Data space extension by literature data, physics based simulations, image and other monitoring data to guarantee reproducible processing is recommended.

4. Conclusions

Knowledge- and physics based process – property correlation is of high demand in magnesium sheet manufacturing. Here, an efficient machine learning framework is suggested to facilitate intelligent sheet manufacturing. In a test scenario for magnesium alloy AZ31 despite the complex interdependencies of processing parameters, we illustrated that machine learning has a high potential for sheet property prediction. Application of the algorithm in order to predict pole figures (data) from stress-strain curve measurements and two processing parameters shows good correlation with respect to the data. The developed algorithm applies dimensionality reduction, a feedforward neural network, BAYESian regularization including precise error minimization and analysis, and allows to look for correlation within very limited data spaces. If we take a look into the future the approach might be used to create efficient manufacturing data spaces enabling intelligent processing routes and Industry 5.0.

Acknowledgment

Data availability

The raw data required to reproduce these findings are available to download from [https://github.com/mrshariati/Mg-sheet-machine-learning-algorithm]. The processed data required to reproduce these findings are available to download from [https://github.com/mrshariati/Mg-sheet-machine-learning-algorithm].

CRediT authorship contribution statement

Mohamadreza Shariati: ML Methodology, Software, Writing. **Wolfgang E. Weber:** Data interpretation, Writing. **Jan Bohlen:** Data interpretation, Writing. **Gerrit Kurz:** Experimental data, Data evaluation, Writing. **Dietmar Letzig:** Conceptualization of this study. **Daniel Höche:** Con-

ceptualization of this study, Data curation, Writing - Original draft preparation.

References

[1] Aljarrah, M., Essadiqi, E., Kang, D., Jung, I.H., 2011. Solidification microstructure and mechanical properties of hot rolled and annealed mg sheet produced through twin roll casting route. Materials Science Forum 690, 331–334. doi:10.4028/www.scientific.net/MSF.690.331.

[2] Bachmann, F., Hielscher, R., Schaeben, H., 2010. Texture analysis with mtex - free and open source software toolbox. Solid State Phenomena 160, 63–68.

[3] Basson, F., Letzig, D., 2010. Aluminium twin roll casting transfers benefits to magnesium. Aluminium International Today , 19–21.

[4] Bishop, C.M., 1995. Bayesian Methods for Neural Networks. Technical report ed., Aston University, Birmingham.

[5] Bohlen, J., Kurz, G., Yi, S., Letzig, D., 2012. Rolling of magnesium alloys, in: Advances in Wrought Magnesium Alloys. Elsevier, pp. 346–375.

[6] Chino, Y., Mabuchi, M., 2009. Enhanced stretch formability of mg–al–zn alloy sheets rolled at high temperature (723 k). Scripta Materialia 60, 447–450.

[7] Foresee, F.D., Hagan, M.T., 1997. Gauss-newton approximation to bayesian learning. Proceedings of International Conference on Neural Networks (ICNN'97) 3, 1930–1935. doi:10.1109/ICNN.1997.614194.

[8] Haykin, S.S., 2009. Neural Networks and Learning Machines. 3th ed., Pearson.

[9] Jeong, H.T., Ha, T.K., 2007. Texture development in a warm rolled az31 magnesium alloy. Journal of Materials Processing Technology 187, 559–561.

[10] Jin, L., Dong, J., Wang, R., Peng, L., 2010. Effects of hot rolling processing on microstructures and mechanical properties of mg–3% al–1% zn alloy sheet. Materials Science and Engineering: A 527, 1970–1974.

[11] Kawalla, R., Oswald, M., Schmidt, C., Ullmann, M., Vogt, H.P., Cuong, N.D., 2008. Development of a strip-rolling technology for mg alloys based on the twin-roll-casting process. TMS Magnesium Technology , 177–182.

[12] Kleiner, M., Curbach, M., Tekkaya, A.E., Ritter, R., Speck, K., Trompeter, M., 2008. Development of ultra high performance concrete dies for sheet metal hydroforming. Production Engineering 2, 201–208. doi:10.1007/s11740-008-0099-z.

[13] Kree, V., Bohlen, J., Letzig, D., Kainer, K., 2004. The metallographical examination of magnesium alloys. Practical Metallography 5, 233–246.

[14] Kurz, G., Bohlen, J., Letzig, D., Kainer, K., 2013. Influence of process parameters on twin roll cast strip of the alloy az31. Materials Science Forum 765, 205–209. doi:10.4028/www.scientific.net/MSF.765.205.

[15] Kurz, G., Pakulat, S., Bohlen, J., Letzig, D., 2015. Rolling twin roll cast magnesium strips with varied temperature and degree of deformation. Materials Today. Proceedings 2S, 39–44.

[16] van der Maaten, L.J.P., 2007. An Introduction to Dimensionality Reduction Using Matlab - Bayesian Methods for Neural Networks. Report MICC 07-07 ed., MICC, Maastricht University.

[17] Nestler, K., Bohlen, J., Letzig, D., Kainer, K.U., 2007. Influence of process parameters on the mechanical properties of rolled mangnesium zm21-sheets. Magnesium Technology 2007 , 95–100.

[18] Park, S.S., Bae, G.T., Lee, J.G., Kang, D.H., Shin, K.S., Kim, N.J., 2007. Microstructure and mechanical properties of twin-roll strip cast mg alloys. Materials Science Forum 539/543, 119–126.

[19] Roweis, S.T., Saul, L.K., 2000. Nonlinear dimensionality reduction by locally linear embedding. Science 290, 2323–2326. doi:10.1126/science.290.5500.2323.

[20] St John, D.H., 2007. Overview of current international magnesium research and recent cast crc developments. Advanced Materials Research 29-30, 3–8.

[21] Victoria-Hernandez, J., Yi, S., Bohlen, J., Kurz, G., Letzig, D., 2014. The influence of the recrystallization mechanisms and grain growth on the texture of a hot rolled az31 sheet during subsequent isochronal annealing. Journal of Alloys and Compounds 616, 189–197.

[22] Watari, H., Haga, T., Paisarn, R., Koga, N., Davey, K., 2007. Mechanical properties and metallurgical qualities of sheets manufactured by twin-roll casting. Key Engineering Materials 345/346, 165–168.

[23] Weber, W.E., Reuter, U., 2017. Fuzzy modeling of wave-shielding under consideration of cost-effectiveness for an efficient reduction of uncertainty. Advances in Engineering Software 109, 53–61. doi:10.1016/j.advengsoft.2017.03.005.